Обзор ArXiv/astro-ph, 17-23 мая 2018 года

От Сильченко О.К.

Astro-ph: 1805.05964

KINETyS II: Constraints on spatial variations of the stellar initial mass function from K-band spectroscopy ★

P. D. Alton,[1]† R. J. Smith,[1] and J. R. Lucey,[1]
[1] *Centre for Extragalactic Astronomy, Department of Physics, Durham University, South Road, Durham DH1 3LE, UK*

Accepted 2018 May 4th. Received 2018 April 7; in original form 2017 July 12.

ABSTRACT

We investigate the spatially resolved stellar populations of a sample of seven nearby massive Early-type galaxies (ETGs), using optical and near infrared data, including K-band spectroscopy. This data offers good prospects for mitigating the uncertainties inherent in stellar population modelling by making a wide variety of strong spectroscopic features available. We report new VLT-KMOS measurements of the average empirical radial gradients out to the effective radius in the strengths of the Ca I 1.98 µm and 2.26 µm features, the Na I 2.21 µm line, and the CO 2.30 µm bandhead. Following previous work, which has indicated an excess of dwarf stars in the cores of massive ETGs, we pay specific attention to radial variations in the stellar initial mass function (IMF) as well as modelling the chemical abundance patterns and stellar population ages in our sample. Using state-of-the-art stellar population models

Объекты, которые сложили

Table 1. List of sample galaxies with observation details and key properties listed. Effective radii and total (J-band) magnitudes within the effective radius were extracted from 2MASS J-band images and used to calculate the mean surface brightness. Recession velocities were derived using pPXF and $\sigma(R_{eff}/8)$ values and fast/slow rotator status were taken from the ATLAS 3D survey (except for NGC 1407 for which a value was derived from our pPXF fits). Relative M/L taken from CvD12b.

Name	Seeing arcsec	observation time sec	R_{eff} arcsec	cz kms^{-1}	$\sigma(R_{eff}/8)$ kms^{-1}	surface brightness mag_J $arcsec^{-2}$	relative M/L (Milky Way = 1)	ellipticity	Notes
NGC 1407	0.68–0.75	1440	36.2	1950	301	17.4	—	0.00	Slow rotator
NGC 3377	0.88–1.16	2880	23.3	690	146	17.0	1.16	0.40	Fast rotator
NGC 3379	0.95–1.24	2880	28.5	900	213	16.5	1.60	0.00	Fast rotator
NGC 4486	0.99–1.34	2880	44.5	1290	314	16.9	1.90	0.00	Slow rotator
NGC 4552	0.89–1.07	2880	24.1	390	262	16.6	2.04	0.00	Slow rotator
NGC 4621	1.02–1.22	1440	27.7	480	224	16.8	1.96	0.33	Fast rotator
NGC 5813	1.13–1.57	2880	33.7	1920	226	17.9	1.37	0.25	Slow rotator

Индексы, которые моделировали

Table 2. List of absorption index names and definitions (vacuum wavelength definitions, given in Å); originally from CvD12a.

Index Name	Blue continuum	Feature Definition	Red continuum	Notes
Hβ	4827.9–4847.9	4847.9–4876.6	4876.6–4891.6	ATLAS^{3D} data
Fe 5015Å	4946.5–4977.8	4977.8–5054.0	5054.0–5065.3	
Mgb	5142.6–5161.4	5160.1–5192.6	5191.4–5206.4	
Na I (0.82 µm)	8170.0–8177.0	8177.0–8205.0	8205.0–8215.0	Paper I data
Ca II (0.86 µm a)	8484.0–8513.0	8474.0–8484.0	8563.0–8577.0	
Ca II (0.86 µm b)	8522.0–8562.0	8474.0–8484.0	8563.0–8577.0	
Ca II (0.86 µm c)	8642.0–8682.0	8619.0–8642.0	8700.0–8725.0	
Mg I (0.88 µm)	8801.9–8816.9	8777.4–8789.4	8847.4–8857.4	
FeH (0.99 µm)	9905.0–9935.0	9855.0–9880.0	9940.0–9970.0	
Ca I (1.03 µm)	10337–10360	10300–10320	10365–10390	
Na I (1.14 µm)	11372–11415	11340–11370	11417–11447	
K I (1.17 µm a)	11680–11705	11667–11680	11710–11750	
K I (1.17 µm b)	11765–11793	11710–11750	11793–11810	
K I (1.25 µm)	12505–12545	12460–12495	12555–12590	
Al I (1.31 µm)	13115–13165	13090–13113	13165–13175	
Ca I (1.98 µm a)	19740–19765	19770–19795	19800–19840	new KMOS data
Ca I (1.98 µm b)	19800–19840	19845–19880	19885–19895	
Na I (2.21 µm)	22035–22045	22047–22105	22107–22120	
Ca I (2.26 µm)	22500–22575	22580–22700	22705–22780	
CO (2.30 µm a)	22860–22910	22932–22982	23020–23070	
CO (2.30 µm b)	23150–23200	23220–23270	23300–23350	

Новые спектры в области 2 мкм

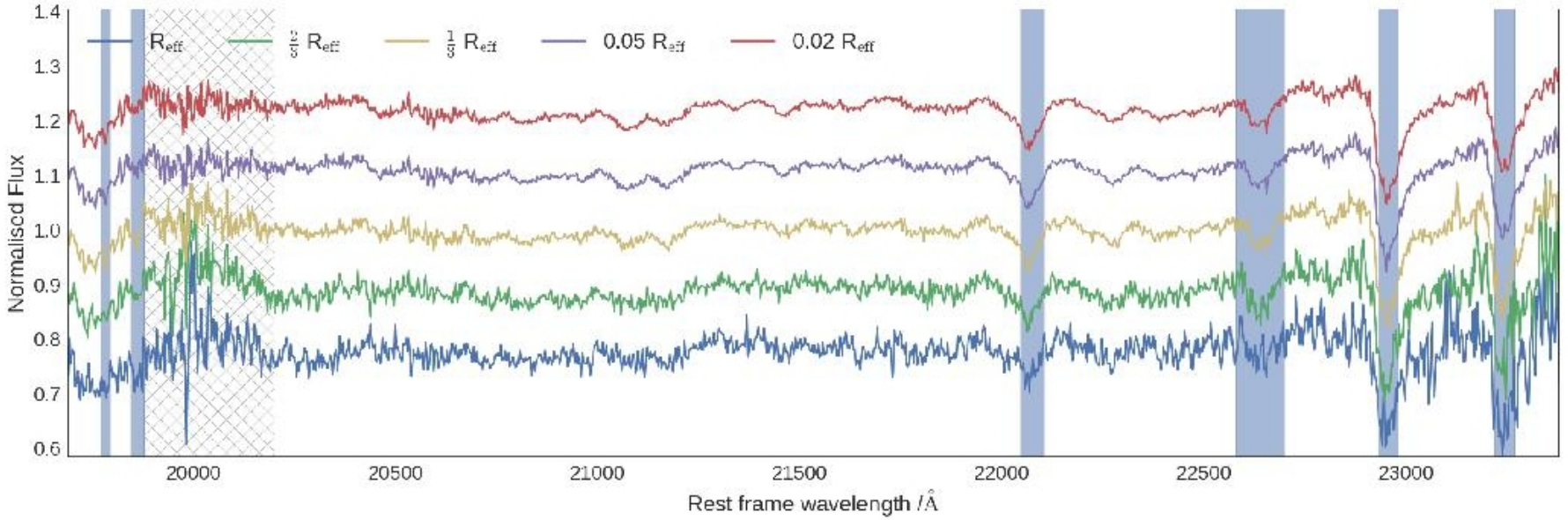

Новые градиенты

Table 3. Best-fit radial gradients (change in equivalent width per decade in radius) derived from the KMOS stacks.

Feature	best-fit gradient (Å) per dex in $\log(R/R_{eff})$
Ca I 1.98 μm	0.05±0.02
Na I 2.21 μm	–0.53±0.08
Ca I 2.26 μm	–0.08±0.09
CO 2.30 μm *a*	–0.11±0.13

Картинка к ним

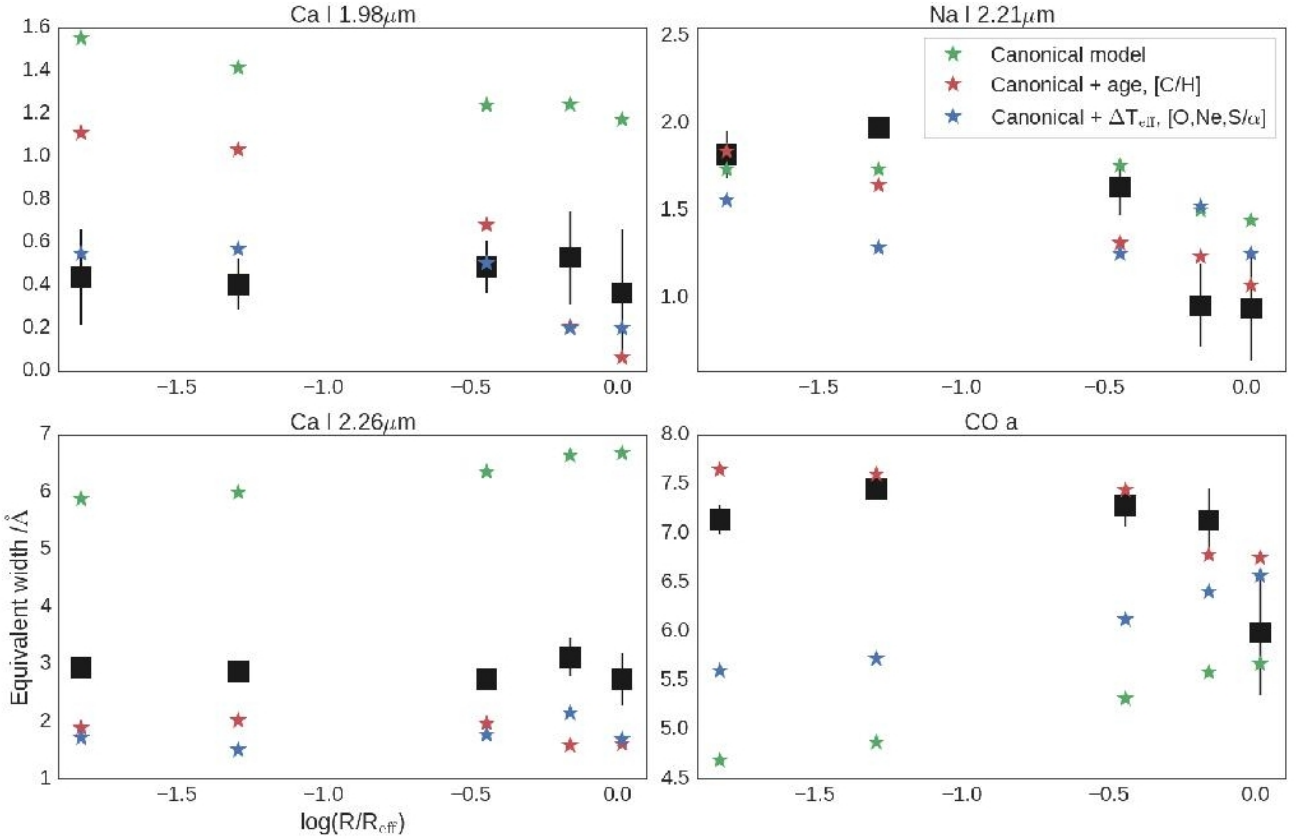

Figure 2. Measurements from the stacked KMOS K-band spectra with errors (large black symbols). Also shown are the predictions of the best-fit models from Paper I, which were *not* constrained using these data (i.e. these are true predictions).
Green: the 'canonical model' of Paper I (which accounts for [α/H], [Fe/H], [Na/H], [Ca/α], [K/H], as well as the IMF).

Параметры звездного населения

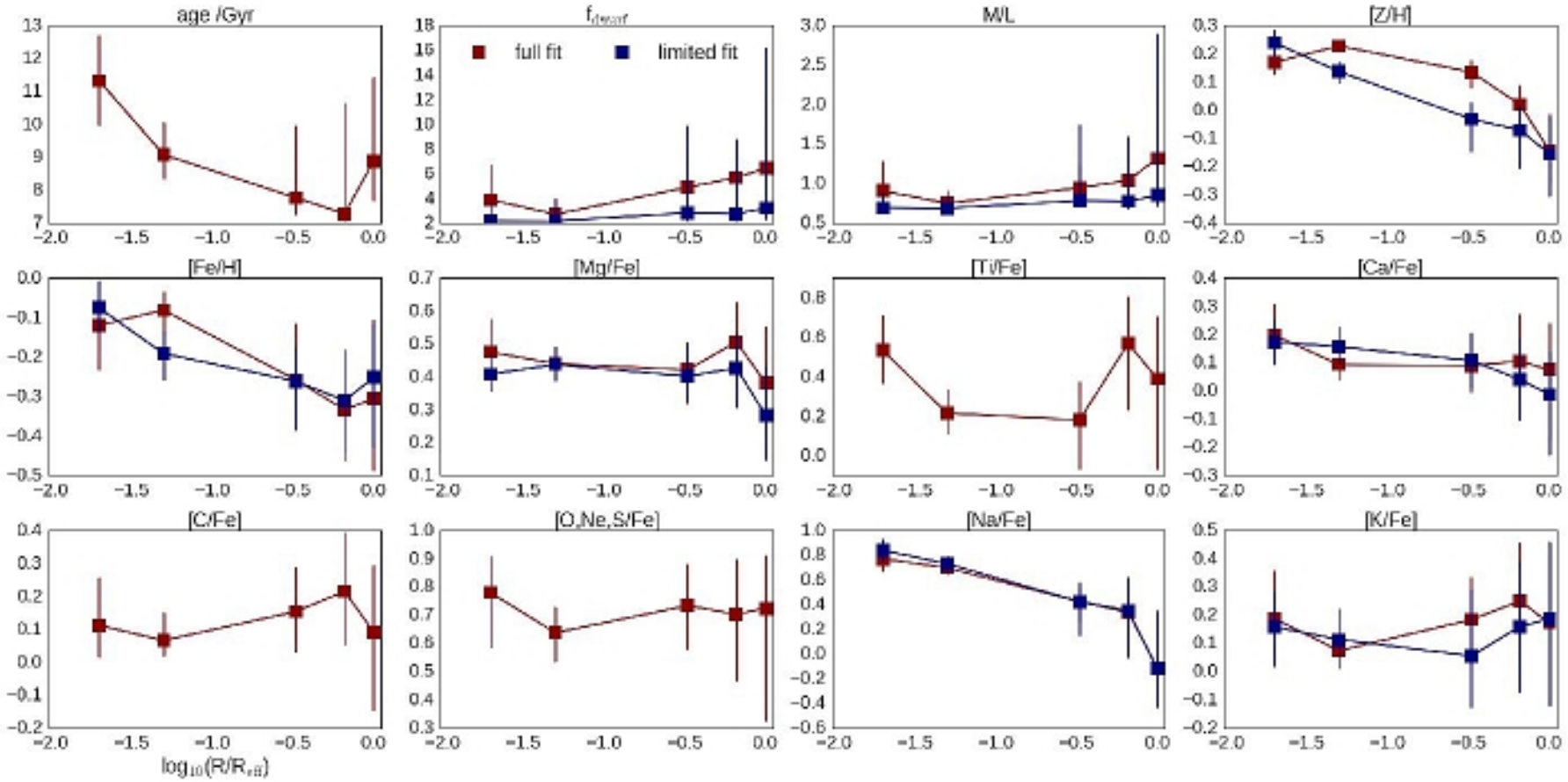

Figure 5. Parameter radial variations via two model fits. The parameters inferred from the stacked spectra using only a limited set of indices and a restricted parameter set are shown in blue, while those inferred when data from the K-band and Hβ and additional model parameters are included are shown in red. Generally, as expected, our results are not radically altered with respect to those obtained previously, although the best-fit [Z/H] is an exception.

Особый нуклеосинтез натрия в центре массивных E-галактик

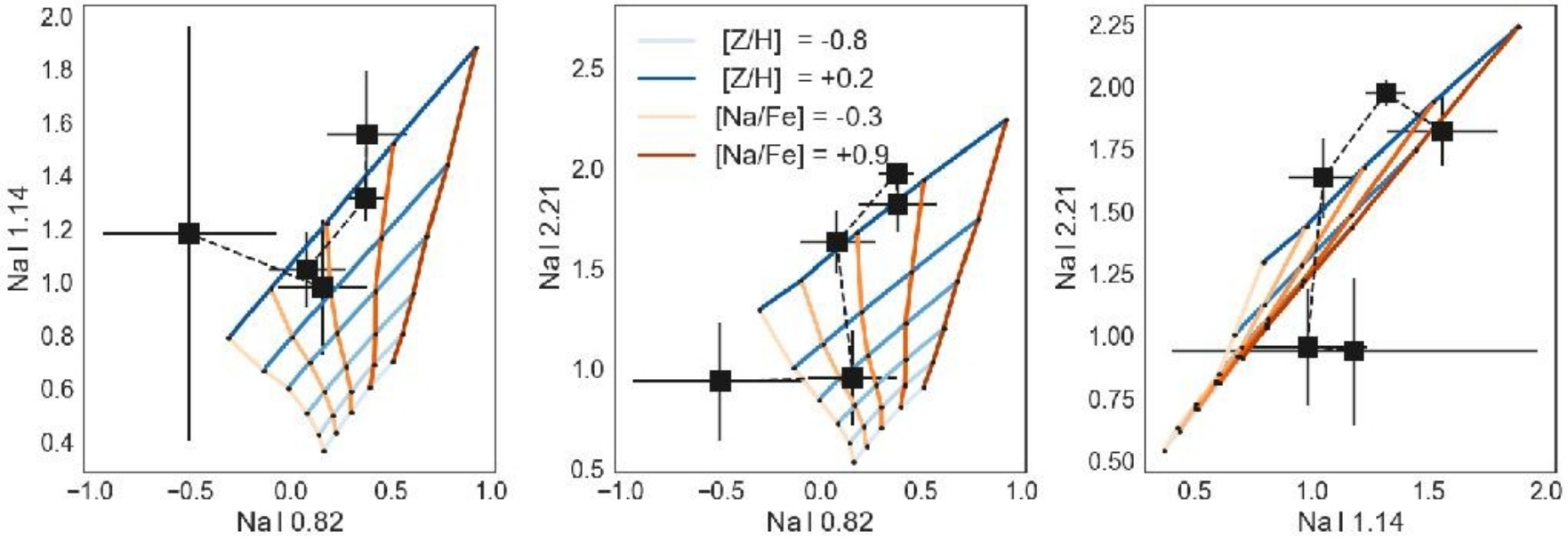

Figure 10. Equivalent widths of the Na features, measured on the stacked spectra, along with model grids where the vertices indicate variation of metallicity and [Na/Fe], assuming a Milky Way-like IMF. Blue lines are lines of constant [Z/H], orange lines are lines of constant [Na/Fe]. Darker colours indicate higher values. Finally, dashed lines link data points from adjacent radial extraction zones.

Выводы

(i) We used stacked spectra extracted from different radii within the KINETyS sample to investigate the radial behaviour of four K-band spectral features. We found a strong decline in the strength of the Na I 2.21μm line with radius (-0.53 ± 0.08 per decade in R/R_{eff}), and fairly constant strength for two Ca I features. The CO 2.30 μm *a* line likewise appears roughly constant in strength (-0.11 ± 0.13).

(ii) We use our updated stellar population spectral index fitting code in conjunction with these measurements to place additional constraints on the stellar populations of our sample. From the stacked spectra we recover an average metallicity gradient Δ[Z/H] of -0.11 ± 0.03 per decade in R/R_{eff} and measure the abundances of several α-capture elements, finding flat trends in the relative abundances [Mg/Fe], [Ca/Fe], [Ti/Fe], and [O, Ne, S/Fe]. The latter two parameters are not well constrained, but we find [Ca/Fe] much less enhanced than [Mg/Fe], consistent with our previous findings.

(iii) We find a very strong radial gradient in [Na/Fe] of -0.35 ± 0.09, a tighter constraint than that presented in Paper I, aided by our measurements of the Na I 2.21μm line. However, there is mild tension between the absolute strengths of the three Na I features we measure, which may be a consequence of the theoretical modelling of Na line strengths in stellar populations where Na is superabundant. The ex-

IMF=Milky-Way like, non varying radially

Nature - astro-ph:1805.05966

The onset of star formation 250 million years after the Big Bang

Takuya Hashimoto[*,1,2], Nicolas Laporte[3,4], Ken Mawatari[1], Richard S. Ellis[3], Akio. K. Inoue[1], Erik Zackrisson[5], Guido Roberts-Borsani[3], Wei Zheng[6], Yoichi Tamura[7], Franz E. Bauer[8,9,10], Thomas Fletcher[3], Yuichi Harikane[11,12], Bunyo Hatsukade[13], Natsuki H. Hayatsu[12,14], Yuichi Matsuda[2,15], Hiroshi Matsuo[2,15], Takashi Okamoto[16], Masami Ouchi[11,17], Roser Pelló[4], Claes-Erik Rydberg[18], Ikkoh Shimizu[19], Yoshiaki Taniguchi[20], Hideki Umehata[13,20,21], Naoki Yoshida[12,17]

Abstract

The abundance of star-forming galaxies is known to decline[4,5] from redshifts of about 6 to 10, but a key question is the extent of star formation at even earlier times, corresponding to the period when the first galaxies might have emerged. Here we present spectroscopic observations of MACS1149-JD1[6], a gravitationally lensed galaxy observed when the Universe was less than four per cent of its present age. We detect an emission line of doubly ionized oxygen at a redshift of 9.1096±0.0006, with an uncertainty of one standard deviation. This precisely determined redshift indicates that the red rest-frame optical colour arises from a dominant stellar component that formed about 250 million years after the Big Bang, corresponding to a redshift of about 15. Our results indicate the it may be possible to detect such early episodes of star formation in similar galaxies with future telescopes.

Данные ALMA в линии [OIII]88 мкм

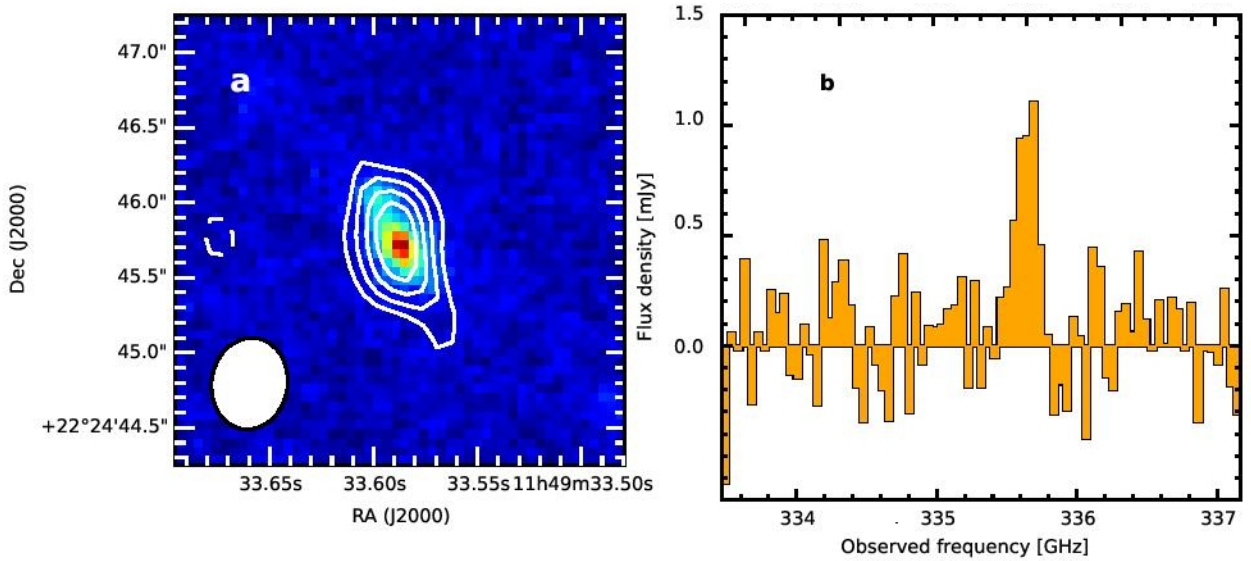

Figure 1 | ALMA [OIII] contours and spectrum of MACS1149-JD1. (a) Zoom on an *HST* image

Характеристики объекта

Table 1| Properties of MACS1149-JD1.

Parameters	Values
RA	$11:49:33.58$
Dec	$+22:24:45.7$
Redshift $z_{[\mathrm{OIII}]}$	9.1096 ± 0.0006
[OIII] line width FWHM$_{[\mathrm{OIII}]}$ (km s^{-1})	154 ± 39
[OIII] luminosity $L_{[\mathrm{OIII}]}$ (10^7 $L_\odot$)	$(7.4 \pm 1.6) \times (10/\mu)^a$
90 μm continuum flux (μJy beam^{-1})	$< 5.3 \times (10/\mu)^a$ (3σ)
Star formation rate ($M_\odot$ yr^{-1})	$4.2^{+0.8}_{-1.1} \times (10/\mu)^a$
Stellar mass ($10^9 M_\odot$)	$1.08^{+0.53}_{-0.18} \times (10/\mu)^a$
Dust mass (10^5 $M_\odot$)	$< 5.2 \times (10/\mu)^a$ (3σ)^b
Dynamical mass ($10^9 M_\odot$)	$(4 \pm 3) \times (10/\mu)^{0.5}$ ^{a,c}
Redshift $z_{\mathrm{Ly}\alpha}$	9.0944 ± 0.0019
Velocity offset $\Delta v_{\mathrm{Ly}\alpha}$ (km s^{-1})	-450 ± 60
Lyα line width FWHM$_{\mathrm{Ly}\alpha}$ (km s^{-1})	144 ± 56
Lyα luminosity $L_{\mathrm{Ly}\alpha}$ (10^7 $L_\odot$)	$(12.4 \pm 3.2) \times (10/\mu)^a$

[a] μ is the lensing magnification

[b] We assume dust temperature $T_\mathrm{d} = 40$ K, spectral index $\beta_\mathrm{d} = 1.5$, and the dust emitting region of a single beam size

[c] The value under the assumption that lensing effects are equal for the major and minor axes

Линия= current SF, SED=относительно старый возраст

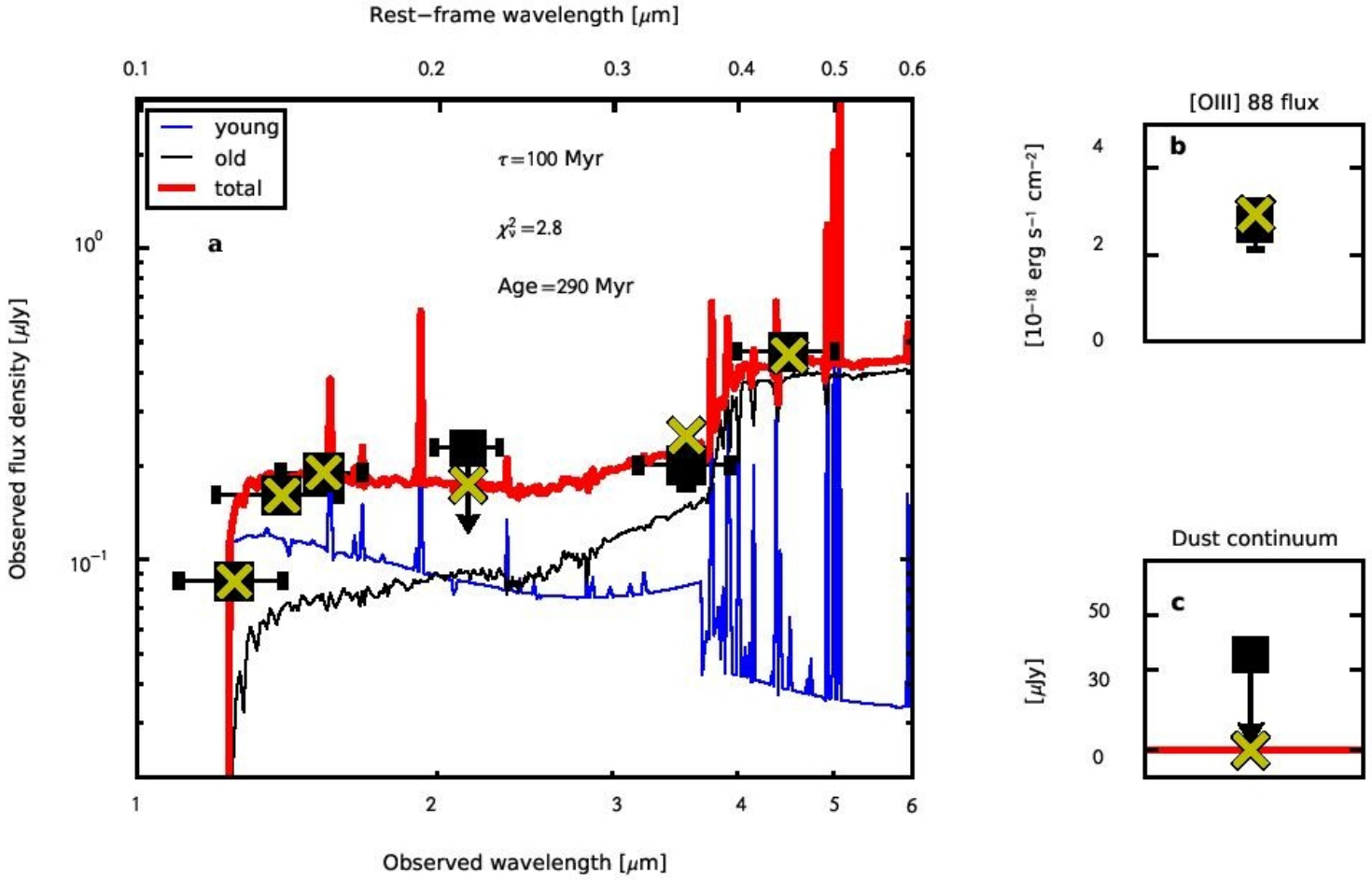

Astro-ph: 1805.05970

TIDAL FEATURES AT $0.05 < z < 0.45$ IN THE HYPER SUPRIME-CAM SUBARU STRATEGIC PROGRAM: PROPERTIES AND FORMATION CHANNELS

E. Kado-Fong[1], J. E. Greene [1], D. Hendel [2], A. M. Price-Whelan [1], J. P. Greco [1], A. D. Goulding [1], S. Huang [3,4], K. V. Johnston [2], Y. Komiyama [5,6] C.-H. Lee [7], N. B. Lust [1], M. A. Strauss [1], M. Tanaka [5]

(Dated: May 17, 2018)

[1]Department of Astrophysical Sciences, Princeton University, Princeton, NJ 08544, USA

[2]Department of Astronomy, Columbia University, 550 W 120th St, New York, NY 10027, USA

[3]Kavli-IPMU, The University of Tokyo Institutes for Advanced Study, the University of Tokyo, Kashiwa 277-8583, Japan

[4]Department of Astronomy and Astrophysics, University of California Santa Cruz, 1156 High St., Santa Cruz, CA 95064, USA

[5]National Astronomical Observatory of Japan, 2-21-1 Osawa, Mitaka, Tokyo 181-8588, Japan

[6]Graduate University for Advanced Studies (SOKENDAI), 2-21-1 Osawa, Mitaka, Tokyo 181-8588, Japan

[7]Subaru Telescope, NAOJ, 650 North A'ohoku Place, Hilo, HI 96720, USA

ABSTRACT

We present 1,201 galaxies at $0.05 < z < 0.45$ that host tidal features, detected from the first ~ 200 deg^2 of imaging from the Hyper Suprime-Cam Subaru Strategic Program (HSC-SSP). All galaxies in the present sample have spectroscopic observations from the Sloan Digital Sky Survey (SDSS) spectroscopic campaigns, generating a sample of 21,208 galaxies. Of these galaxies, we identify 214 shell systems and 987 stream systems. For 575 of these systems, we are additionally able to measure the $(g-i)$ colors of the tidal features. We find evidence for star formation in a subset of the streams, with the exception of streams around massive ellipticals, and find that stream host galaxies span the full range of stellar masses in our sample. Galaxies which host shells are predominantly red

Морфология оболочек и потоков

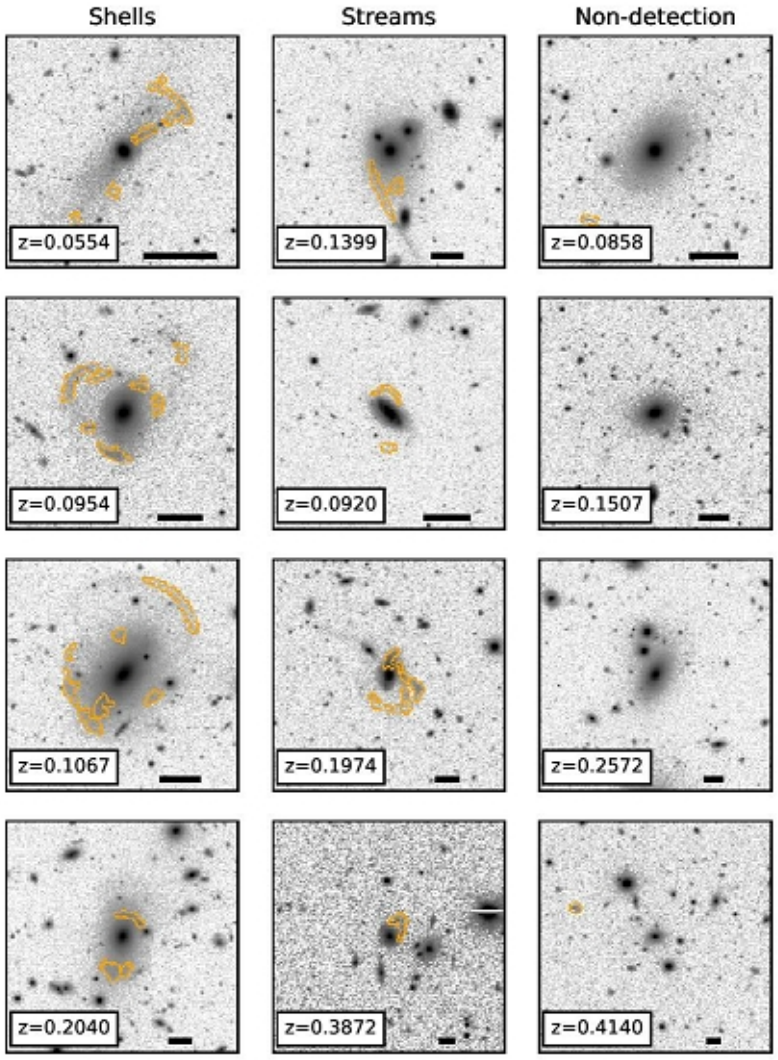

Figure 5. A sample of $i_{\rm HSC}$ band imaging of shells (left column), streams (middle column) and non-interacting galaxies (right) in our sample. The orange outlines show the boundaries of the detected regions found by our filtering algorithm. The horizontal black line in the bottom right of each panel spans 30 kpc at the redshift of the central galaxy. In all panels, a logarithmic stretch is used to emphasize low surface brightness features.

Встречаемость оболочек и потоков

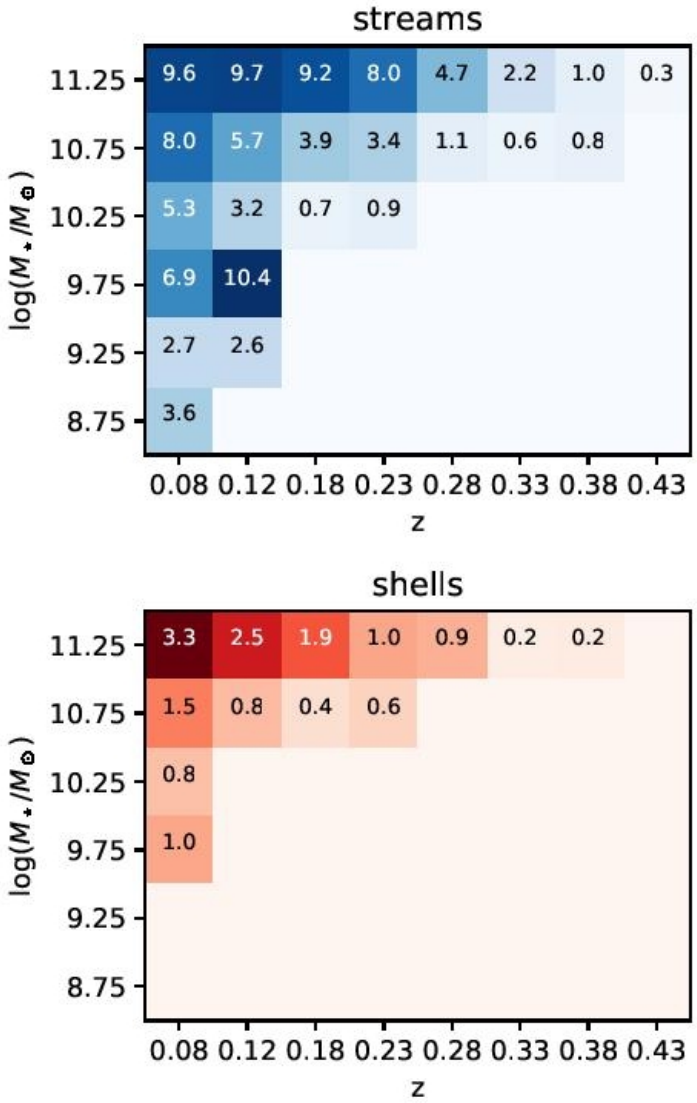

Цвет – по отношению к родительской галактике и restframe

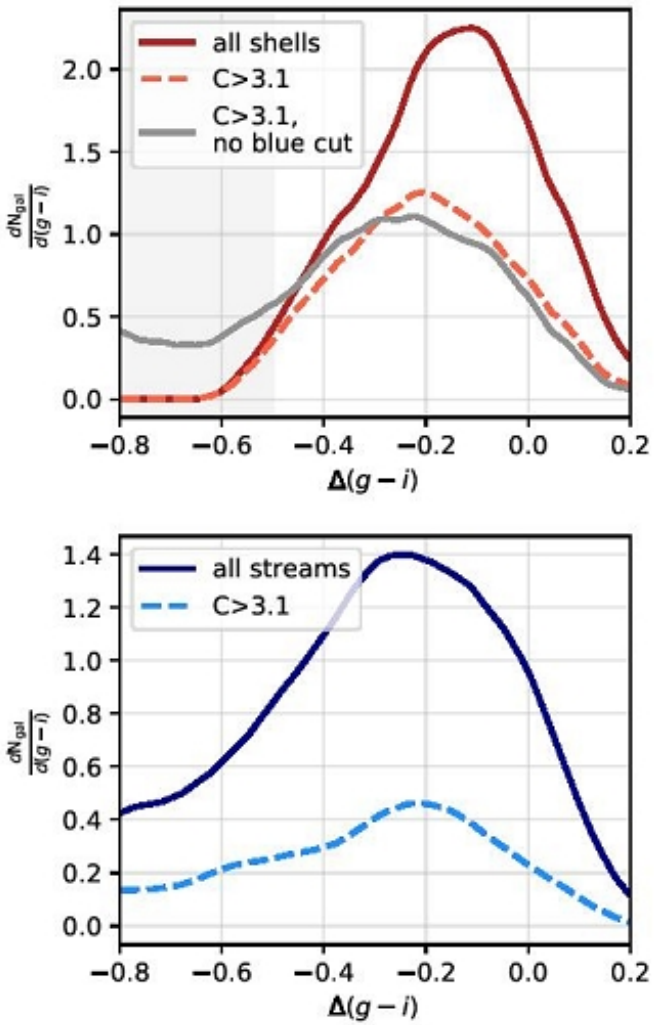

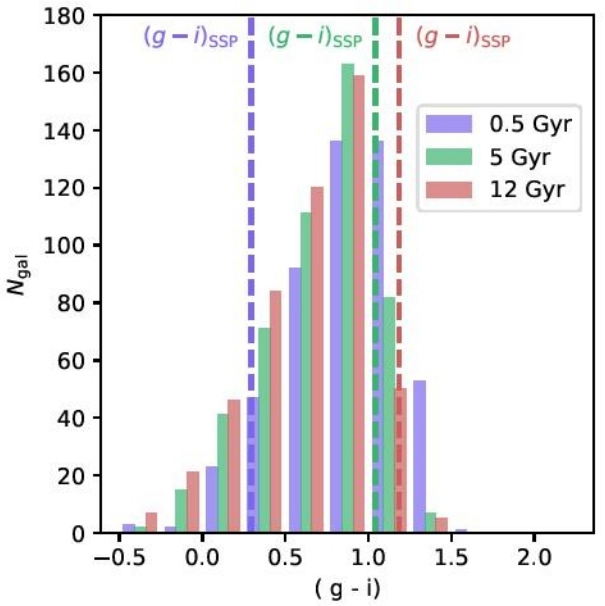

Figure 11. The distribution of $(g-i)$ restframe colors for our stream sample, using the K-correction computed for a 0.5 Gyr (purple), 5 Gyr (green), and 12 Gyr (red) SSP from Bruzual & Charlot 2003. The dashed vertical lines show the restframe colors for, from left to right, the 0.5 Gyr (purple), 5 Gyr (green) and 12 Gyr (red) populations. The existence of streams with rest-frame colors bluer than the youngest SSP considered implies that a subset of the streams host star formation.

Вывод про оболочки

the full range of stellar masses in our sample. Galaxies which host shells are predominantly red and massive: we find that observable shells form more frequently around ellipticals than around disc galaxies of the same stellar mass. Although the majority of the shells in our sample are consistent with being formed by minor mergers, $15\% \pm 4.4\%$ of shell host galaxies have $(g - i)$ colors as red as their host galaxy, consistent with being formed by major mergers. These "red shell" galaxies are additionally preferentially aligned with the major axis of the host galaxy, as previously predicted from simulations. We suggest that although the bulk of the observable shell population originates from fairly minor mergers, which preferentially form shells that are not aligned with the major axis of the galaxy, major mergers produce a significant number of observable shells.